THERMODYNAMICS AND MECHANICAL ENGINEERING

Dual manipulator system calibration based on virtual constraints

Q. ZHU, X. XIE*, and C. LI

College of Automation, Harbin Engineering University, Harbin 150001, China

Abstract. Calibration is necessary for dual manipulator to complete operational tasks. This paper proposes an effective robot-robot and hand-eye calibration method based on virtual constraints. Firstly, a rotational error model and a translational error model are established based on the relationships between the transformation matrices of the dual manipulator calibration system. Then a poses-alignment method is designed to make the poses of the two robots satisfy the constructed virtual constraints. At the aligned positions, the joint angles of the two robots are saved and used to calculate the values of the variables in the error models. Finally, the robot-robot and hand-eye rotational errors are estimated by an iterative algorithm. These errors are then used to calculate translational errors based on the SVD (singular value decomposition) method. To show the feasibility and effectiveness of the proposed method, experiments of robot-robot and hand-eye calibration for dual manipulators are performed. The experiment results demonstrate that the accuracy of the dual manipulator system is improved greatly.

Key words: dual manipulators, calibration, virtual constraint, optical axis, robot-robot, hand-eye.

1. Introduction

Compared with the single robot, multi-robots demonstrate more evident superiority in most application tasks [1–3]. Dual manipulator system is efficient, small volume and capable of performing multiple complex tasks. At the same time, when performing operational tasks, the dual manipulator system should be accurate enough to guarantee safety. Otherwise, even small errors could induce large interaction forces, which could damage the workpiece or the robots. Therefore, the calibration for dual manipulator system is vitally necessary, a fact which hasn't gained enough concern nowadays.

Most of all, the robot-robot transformation matrix should be calibrated to ensure that the robots perform cooperating tasks. For the dual robot system with a camera, the calibration problem is extended to include robot-robot calibration, hand-eye calibration, tool-flange calibration and robot kinematics calibration. A lot of research has been done on the kinematics calibration of a single robot [4, 5] while calibration of the dual robot system has received little attention. The dual manipulator calibration problem is challenging both theoretically and practically. In fact, direct measurement is unavailable because the origin of the robot base frame is inaccessible. Many studies have addressed the problem as an isolated one, where the robot-world (or sensor-world) calibration is performed separately for each robot. This repeated process generates measurement errors and has a negative effect on the calibration results.

A suitable calibration error model is crucial for applying the robot calibration procedure. The dual manipulator system calibration problem is similar with the hand-sensor and robot-world calibration problem. The latter is well known as the "**AX** = **YB**" problem [6, 7], where **A** (sensor-world) and **B** (robot base-end-effector) are the transformations measured from sensors, and **X** (hand-sensor), **Y** (robot-world) are the unknown transformations to be calibrated. To solve this equation, the values of **A** and **B** are used as inputs of the calculation algorithm based on quaternions [8], dual-quaternions [9], Kronecker product [10] or polynomial optimization [11]. Extended from these formulations, Wu [12] formulated the hand-eye, robot-robot and tool-flange calibrations for dual manipulators as the "**AXB** = **YCZ**" problem, and Ma [13] formulated the multi-robots calibration problem using equation "**AXB** = **YCZ**", too. In these two equations, **A** (base-end-effector of robot 1), **B** (eye-tool), **C** (base-end-effector of robot 2) are the time-varying transformations measured from sensors, and **X** (hand-eye), **Y** (robot-robot) and **Z** (tool-flange) are the unknown static transformations to be calibrated. By solving the established formulation, the unknown transformation matrix **X**, **Y** and **Z** can be calibrated simultaneously.

The accurate values of the robot poses which are measured within the sensor frame are usually needed to solve the formulations above. At the earliest age of research, high precision devices or sensors, such as laser trackers, were used to measure the poses of the robots. These apparatuses are expensive and must be operated by professional personnel. As an alternative, a camera [6, 14–15] is a low-cost device which has been widely used as the sensor to calibrate robot systems. However, the calibration results are usually affected by the camera measurement results, which can't be neglected.

Simple apparatus and elaborate tools [16, 17] like plates and tips were all used as a low-cost solution to the calibration problem. By making the two robots form a closed kinematic chain, the parameters are estimated only using the joint angles, and there is no need to measure the robots' poses. Gan [16] carried out base frame calibration for multi-robots through a series of

"handclasp" operations. The base-base rotational matrix was estimated firstly and then used to calculate the translational vector. Hirsh [19] proposed an iterative approach to calibrating hand-eye and base-world transformations simultaneously. Rotational errors were estimated recursively and then used to estimate translational errors. Wu [20] proposed a closed-form solution and an iterative solution to the hand-eye calibration problem to find the robot base frame.

In this paper, a novel calibration method for dual manipulators based on virtual constraints is proposed. It is cheap, accurate and easy-to-perform. The optical axis of the camera serves as the virtual constraint. The robot-robot and hand-eye transformations are calibrated using only a camera and a common calibration target. The experiments demonstrate that the accuracy of the dual manipulator system is improved greatly.

The novelties and advantages of the proposed method are as follows: (1) a novel rotational error model and translational error model are established, respectively, based on the virtual line constraint. The actual poses of the robot in the camera frame are not needed in our error model, which avoids the negative influences of inaccurate positioning of the camera. (2) During the calibration poses selection process, two constraints are designed to restrict the calibration poses of the robots. (3) In the data measurement process, an automatic feature point alignment algorithm is designed. (4) An iterative estimation algorithm is designed to estimate rotational errors and the SVD method is used to estimate translational errors.

The rest of the paper is organized as follows: Section 2 introduces the main idea and scheme of the proposed calibration method. Section 3 formulates the calibration problem and establishes a rotational error model and a translational error model. The calibration poses selection and data measurement processes are described in Section 4. Section 5 presents the error estimation algorithms and the validation method. The experiments and results are illustrated in Section 6. Finally, discussion and conclusion are offered in Section 7 and 8, respectively.

2. Calibration methodology

The kinematic parameters and tool-flange transformation matrix of the dual manipulator system have been calibrated in our previous work [21]. This paper addresses calibration of the base-base homogeneous transformation of two cooperative manipulators. Meanwhile, the hand-eye relative position and the optical axis vector of the camera in the hand frame are calibrated simultaneously.

The calibration devices used in this paper refer to a camera and a calibration target. The calibration technique is performed on the two robots. One of the robots is equipped with a camera mounted in eye-in-hand configuration, and is referred to hereinafter as the "active robot". The other one has a calibration target attached to its end effector, and is referred to hereinafter as the "passive robot". The frames of the dual manipulator calibration system are shown in Fig. 1. The tool center point (TCP) on the calibration target serves as a feature point, and it is supposed to be visible for the camera.
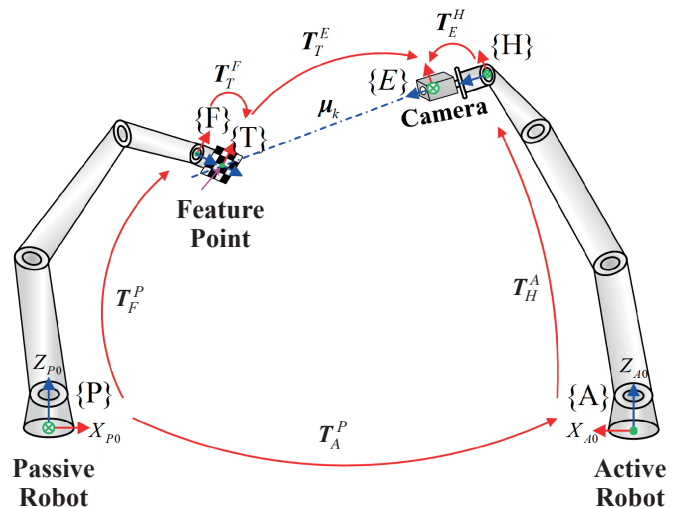

Fig. 1. Relative frames and transformation of the dual manipulator system

The calibration method proposed in this paper is based on virtual constraints which are constructed by the optical axis of the camera. In the calibration procedure, virtual constraints are constructed by controlling the active robot to assume different poses. At each pose of the active robot, the feature point attached to the passive robot is controlled to satisfy the virtual constraint at several positions. On the one hand, the optical axis vector μ_k in the base frame of the passive robot can be estimated using the actual positions of the feature point, which is related to T_F^P and T_T^F. On the other hand, the reconstructed optical axis vector μ_k' in the base frame of the passive robot can be calculated by the Z-axis of the camera, which is related to T_A^P, T_H^A and T_E^H. Because of the errors in T_A^P and T_E^H, the reconstructed optical axis vector μ_k' mismatches with μ_k. The errors between μ_k and μ_k' are used to estimate the errors of T_A^P and T_E^H through an iterative algorithm.

The calibration procedure of the dual manipulator system, including robot-robot and hand-eye calibration, is divided into three steps: 1) error model establishment, 2) data measurement, and 3) error estimation. The scheme of the calibration procedure is shown in Fig. 2. The details of these three steps are illustrated in the following sections.

3. Calibration error model

In this part, a rotational calibration error model and a translational calibration error model are established, respectively, based on the relationship of the dual robot calibration system. Rotational errors refer to the errors of base-base rotational matrix and the Z-axis vector of the camera in the hand frame. Translational errors refer to the errors of base-base translational vector and hand-eye translational vector.

3.1. Rotational error model. According to the rotation relationship of the dual manipulator system, the Z-axis direction
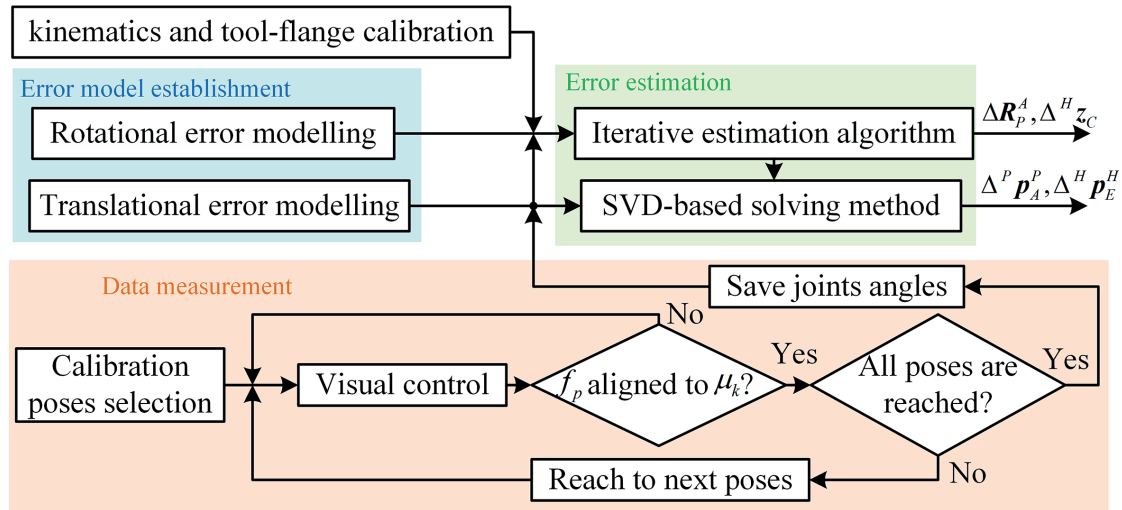
Fig.2. Scheme of the proposed calibration method

vector of the camera in the base coordinates of the active robot $^A z_E$ can be formulated as follows:

$$^A z_E = R_P^A \, ^P z_E = R_H^A \, ^H z_E. \tag{1}$$

$^P z_E$ can be estimated from the actual positions of the feature point, and R_H^A can be calculated by the kinematics of the active robot. The base-base rotation matrix R_P^A and vector $^H z_E$ are unknown. By applying the errors of R_P^A and $^H z_E$, (1) could be reformulated as:

$$(\overline{R}_P^A + \Delta R_P^A)\, ^P z_E = R_H^A(^H \overline{z}_E + \Delta \, ^H z_E), \tag{2}$$

which could also be written as:

$$\Delta R_P^A \, ^P z_E - R_H^A \Delta \, ^H z_E = R_H^A \, ^H \overline{z}_E - \overline{R}_P^A \, ^P z_E. \tag{3}$$

By using the error model (3), it is possible to devise an iterative algorithm to estimate ΔR_P^A and $\Delta \, ^H z_E$.

3.2. Translational error model. According to the position relationships of the dual manipulator system, the translational vectors in the base coordinates of the passive robot could form a transformation loop. It is formulated as:

$$^P p_E^H + \, ^P p_H^A + \, ^P p_A^P = \, ^P p_E^T + \, ^P p_T^F + \, ^P p_F^P, \tag{4}$$

which could also be written as:

$$R_A^P R_H^A \, ^H p_E^H + R_A^P \, ^A p_H^A + \, ^P p_A^P = \, ^P p_E^T + R_F^P \, ^F p_T^F + \, ^P p_F^P. \tag{5}$$

Considering errors in $^P p_A^P$ and $^H p_E^H$, (5) can be written as the error formulation:

$$R_A^P R_H^A \, ^H \overline{p}_E^H + R_A^P R_H^A \Delta \, ^H p_E^H + R_A^P \, ^A p_H^A + \, ^P \overline{p}_A^P + \Delta \, ^P p_A^P$$
$$= \, ^P p_E^T + R_F^P \, ^F p_T^F + \, ^P p_F^P. \tag{6}$$

Note that $^P p_E^T$ denotes the vector from the origin of the camera frame to the feature point and it is immeasurable in the current method. It has to be eliminated from the error model. The optical axis vector μ_k can be estimated using the actual positions of the feature point. Define operator $[\mu_k \times]$ as: $[\mu_k \times]N = \mu_k \times N$, where N is a 3×1 constant vector. Noticing that $[\mu_k \times]^P p_E^T = 0$, we get:

$$[\mu_k \times](R_A^P R_H^A \, ^H \overline{p}_E^H + R_A^P R_H^A \Delta \, ^H p_E^H + R_A^P \, ^A p_H^A + \, ^P \overline{p}_A^P +$$
$$+ \Delta \, ^P p_A^P) = [\mu_k \times](R_F^P \, ^F p_T^F + \, ^P p_F^P). \tag{7}$$

By further derivation, we have:

$$[\mu_k \times](R_A^P R_H^A \Delta \, ^H p_E^H + \Delta \, ^P p_A^P) = [\mu_k \times](R_F^P \, ^F p_T^F +$$
$$+ \, ^P p_F^P - R_A^P R_H^A \, ^H \overline{p}_E^H - R_A^P \, ^A p_H^A - \, ^P \overline{p}_A^P). \tag{8}$$

Define $col(K, L) = [K^T L^T]^T$, $row(K, L) = [K \, L]$, where K and L are the compatibly dimensional matrices (or vectors). Then (8) can be re-expressed as:

$$J_T^{(i,k)} col(\Delta \, ^P p_A^P, \Delta \, ^H p_E^H] = \rho_T^{(i,k)}, \tag{9}$$

$$J_T^{(i,k)} = [\mu_k \times] row(I, R_A^P R_H^{A(i,k)}), \tag{10}$$

$$\rho_T^{(i,k)} = [\mu_k \times](R_F^{P(i,k)} \, ^F p_T^F + \, ^P p_F^{P(i,k)} -$$
$$- R_A^P R_H^{A(i,k)} \, ^H \overline{p}_E^H - R_A^P \, ^A p_H^{A(i,k)} - \, ^P \overline{p}_A^P). \tag{11}$$

$J_T^{(i,k)}$ is referred to as the translational error's Jacobian matrix at the kth virtual constraint and the ith position of the feature point, and the corresponding $\rho_T^{(i,k)}$ is referred to as the translational error's matrix. For all of the positions of the feature point, we have:

$$J_T col(\Delta \, ^P p_A^P, \Delta \, ^H p_E^H) = \rho_T. \tag{12}$$

J_T is the rank deficient since the error which is co-linear to the optical axis has no influence on ρ_T. By performing singular value decomposition (SVD) of J_T, it is possible to extract the error components.

4. Data measurement

4.1. Calibration poses selection. Prior to the poses alignment process, both robots should assume the calibration poses. The calibration poses selection is crucial to ensure calibration poses' feasibility. In the robot kinematics calibration method, calibration poses optimization is vital to enhance calibration accuracy and kinematic parameters observability [22]. However, calibration poses selection for dual manipulator calibration has received less attention so far. In this Section, the process of the calibration poses selection is presented.

The generated calibration poses of the passive robot (blue circle), corresponding to a calibration pose of the active robot, are shown in Fig. 3. At the calibration poses configurations of the two robots, the calibration target should be in the view of the camera and the feature point should be near the optical axis. Due to the parameters error of the dual robot system, the actual positions (red circle) of the feature point are not on the optical axis exactly once the robots assume the generated calibration poses.
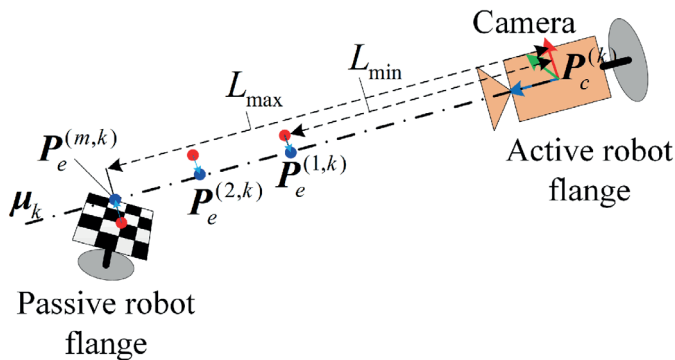

Fig. 3. Generated calibration poses of the passive robot corresponding to a calibration pose of the active robot

The feature point should always be visible during the measurement process. The visibility of the feature point depends on the angle and distance between the camera and the calibration target. Two constraints are constructed to make the calibration poses feasible, i.e. angle constraint and distance constraint.

Define the angle constraint as:

$$C_1 : \alpha_{\min} \leq \alpha_v \leq \alpha_{\max} \tag{13}$$

where α_v is the angle between the optical axis and the calibration target plate while $\alpha_{\min}$ and $\alpha_{\max}$ are the constant values that are determined by the experiments.

Define the distance constraint as:

$$C_2 : L_{\min} \leq L_v \leq L_{\max} \tag{14}$$

where L_v is the distance between the camera and the calibration target plate, L_{min} ensures the whole calibration target's visibility in the camera view, and L_{max} is related to the camera parameters.

The selection process of the robots calibration poses can be divided into four steps:

Step 1. Active robot pose selection.

The pose of the active robot is generated randomly in the whole workspace as long as the optical axis pointing to the workspace of the passive robot. Then the position $P_c^{(k)}$ of the camera and the optical axis vector μ_k in the active robot base frame become known.

Step 2. Passive robot positions selection.

The position $^A P_e^{(i,k)}$ of the feature point in the active robot base frame is:

$$^A P_e^{(i,k)} = P_c^{(k)} + (L_{\min} + iL_{step})\mu_k \tag{15}$$

where $L_{step} = (L_{\max} - L_{\min})/m$ is the distance between two adjacent positions of the feature point, and $m \geq 3$ is the total number of positions of the feature point at each optical axis.

Then the position $^P P_e^{(i,k)}$ in the passive robot base frame is:

$$^P P_e^{(i,k)} = \bar{T}_A^P \, ^A P_e^{(i,k)} \tag{16}$$

where $\bar{T}_A^P$ is the nominal value of the robot's base-base transformation matrix.

Step 3. Passive robot orientations selection.

The orientations of the passive robot are selected randomly as long as α_v satisfies the constructed angle constraint. Then the poses of the passive robot are determined.

Step 4. Repeat Step 1–3 to generate different poses until the number of the calibration poses of the two robots is sufficient. At least three virtual constraints should be constructed to estimate unknown parameters.

4.2. Data measurement. In order to make the positions of the feature point satisfy the optical axis constraint, and to obtain the values of the variables in the error model, a measurement procedure based on the visual control method is performed. Firstly, both robots are controlled to reach the generated calibration poses in sequence. Then a simplified version of the image-based visual control method is used to make the feature point move to the optical axis automatically from the generated calibration poses. Details of poses alignment based on the visual control method are omitted in this paper. Please refer to our previous work [21] for details.

During the poses alignment process, the feature point is supposed to align with the optical axis when the pixel difference between them drop below $(\Delta u_{\max}, \Delta v_{\max})$. The poses alignment error e_c can be calculated based on the relationship between the

image coordinates and the camera coordinates. The coordinates $(x_{1\max}, y_{1\max})$ in the camera frame, which corresponds to the $(\Delta u_{\max}, \Delta v_{\max})$ pixel, are:

$$\begin{cases} x_{1\max} = \dfrac{\Delta u_{\max} \cdot z_1}{k_x} \\[3mm] y_{1\max} = \dfrac{\Delta v_{\max} \cdot z_1}{k_y} \end{cases} \tag{17}$$

where k_x and k_y are the amplification coefficients which can be estimated by means of camera calibration, and z_1 is the distance between the feature point and the camera.

The maximum detection error $e_{c\max}$ is:

$$e_{c\max} = \sqrt{(x_{1\max})^2 + (y_{1\max})^2}. \tag{18}$$

It can be assumed that the poses alignment error has little influence on the dual manipulator calibration result when $e_{c\max}$ is smaller than the repeatability error of the robot.

5. Estimation algorithm

Once the feature point is aligned with the optical axis, the joint angles of each robot are saved. By using the saved angles, the actual poses T_F^P and T_H^A are calculated based on the calibrated kinematics of the two robots. The tool-flange transformation matrix T_T^F is calculated while the calibration target is regarded as the last joint of the passive robot. By using the values of T_T^F and T_F^P, the optical axis vector μ_k can be estimated from the actual positions of the feature point. These values are used to estimate the unknown parameters in the dual manipulator system.

There are two types of errors to be estimated: 1) rotational errors ΔR_P^A and $\Delta^H z_C$ and 2) translational errors $\Delta^P p_A^P$ and $\Delta^H p_E^H$. Rotational errors are estimated recursively and then used to calculate translational errors. The estimation procedure for each type of errors is detailed below. Then the verification method is presented.

5.1. Estimation of rotational errors. In general, solving the rotational error is more challenging because of the nonlinear and normalization natures of the rotation matrix. An error in the rotation matrix R can be modeled as a small rotation δR. By using Rodrigues' formula [23], we arrive at:

$$\delta R = I + \sin(\theta_v)S(v) + (1 - \cos(\theta_v))S(v)S(v), \tag{19}$$

$$S(v) = \begin{bmatrix} 0 & -v_z & v_y \\ v_z & 0 & -v_x \\ -v_y & v_x & 0 \end{bmatrix}, \tag{20}$$

where δR is an orthonormal matrix, $v = [v_x, v_y, v_z]$ is the rotation axis, and θ_v is the rotation angle.

Considering a small error of the rotation matrix, the relationship between the real value R and nominal value $\bar{R}$ can be expressed as:

$$R = \bar{R}\delta R = \Delta R + \bar{R}. \tag{21}$$

Combining (19) and (21), the error term ΔR is obtained from:

$$\Delta R = \bar{R}(\sin(\theta_v)S(v) + (1 - \cos(\theta_v))S(v)S(v)). \tag{22}$$

If the rotation angle θ_v is very small, i.e. $(1 - \cos(\theta_v)) \ll \ll \sin(\theta_v)$, the term $(1 - \cos(\theta_v))S(v)S(v)$ in (22) is negligible because it is quite small compared with ΔR. Then the approximate value is obtained:

$$\Delta R \approx \bar{R}\sin(\theta_v)S(v). \tag{23}$$

It should be noted that the approximation in (23) holds only for small rotation angle θ_v.

The estimation method is inspired by the work presented in [19]. R_P^A is corrected using the iterative estimation results of ΔR_P^A and $\Delta^H z_C$. The principle of the estimation method in this paper is to calculate $\Delta^H z_C$ based on the rotational error model (3) by assuming firstly that ΔR_P^A is equal to $0^{3 \times 3}$. Then the updated $\Delta^H z_C$ is reused to form a regression matrix to calculate ΔR_P^A. When this process is repeated, the estimated errors from different measure results will converge to a reasonable value.

To construct the detailed algorithm, let n be the total number of the virtual constraints. Symbol $\bullet(t)$ denotes the value of the variable $\bullet$ at the tth iteration of the algorithm, and $\bullet^{(k)}$ is the value of the variable $\bullet$ which is calculated using the measurement results at the kth optical axis. The iterative algorithm consists of the following steps:

Step 1. Initialization. $t = 0$, $\Delta R_P^A = 0^{3 \times 3}$.

Step 2. Calculate $\Delta^H z_E$ using measurement results at each optical axis:

$$\Delta^H z_E^{(k)}(t) = (R_H^{A(k)})^T (\bar{R}_P^{A(k)} {}^P z_E^{(k)} - R_H^{A(k)} {}^H \bar{z}_E). \tag{24}$$

Step 3. Calculate and normalize the average value ${}^H \bar{z}_E(t+1)$ from all of $\Delta^H z_E^{(k)}(t)$:

$$^H \bar{z}_E(t+1) = \left({}^H \bar{z}_E(t) + \sum_{k=1}^{n} \Delta^H z_E^{(k)}(t) \right) \Bigg/ \Bigg\| {}^H \bar{z}_E(t) + \\ + \sum_{k=1}^{n} \Delta^H z_E^{(k)}(t) \Bigg\|. \tag{25}$$

Step 4. Calculate $\Delta R_P^A(t)$ using the updated ${}^H \bar{z}_E(t+1)$.
For the dual manipulator system, the error of R_P^A is small. So the rotation angle in (19) is small and formula (23) holds. The error ΔR_P^A is estimated iteratively, so neglecting the term $(1 - \cos(\theta_v))S(v)S(v)$ in (23) has little effect on the estimation result. If we combine (3) and (23), we get:

$$\bar{R}_P^A \theta_v S(v) \, {}^P z_E^{(k)} = R_H^{A(k) \; H} \bar{z}_E(t+1) - \bar{R}_P^{A \; P} z_E^{(k)}. \qquad (26)$$

Let us suppose that $S(w) = \sin(\theta_v) S(v)$, $w = [w_x, w_y, w_z]$ (26) can be expressed as:

$$S(w) \, {}^P z_E^{(k)} = (\bar{R}_P^A)^T R_H^{A(k) \; H} \bar{z}_E(t+1) - {}^P z_E^{(k)}. \qquad (27)$$

Notice that if $S(w) \, {}^P z_E^{(k)} = -\left[{}^P z_E^{(k)} \times \right] w$, we have:

$$J_R^{(k)} w = \rho_R^{(k)} \qquad (28)$$

$$J_R^{(k)} = \left[{}^P z_E^{(k)} \times \right] \qquad (29)$$

$$w(t) = (J_R^T J_R)^{-1} J_R^T \rho_R(t+1). \qquad (30)$$

By using all of the measurement results, we can obtain $J_R = \left[(J_R^1)^T, \cdots, (J_R^n)^T \right]^T$ and $\rho_R = \left[(\rho_R^1)^T, \cdots, (\rho_R^n)^T \right]^T$. Then w is calculated using the following equation:

$$w(t) = (J_R^T J_R)^{-1} J_R^T \rho_R(t+1). \qquad (31)$$

Step 5. Calculate $\delta R_P^A(t)$ and correct $R_P^A(t)$ while guaranteeing its normalization.

$$\delta R_P^A(t) = I + \sin(\theta_v(i)) S(v(i)) + \\ + (1 - \cos(\theta_v(i))) S(v(i)) S(v(i)) \qquad (32)$$

$$\bar{R}_P^A(t+1) = \bar{R}_P^A(t) \delta R_P^A(t), \qquad (33)$$

with $\sin(\theta_v(i)) = \|w(i)\|$, $S(v(i)) = S(w(i)/\sin(\theta_v(i)))$ It is worth noticing that $\delta R_P^A(t)$ rather than $\Delta R_P^A(t)$ is used to update and correct $R_P^A(t)$, so the resulting matrix $\bar{R}_P^A(t+1)$ can be orthonormal.

Step 6. Repeat steps 2–5, until $\left\| \bar{R}_P^A(t+1) - \bar{R}_P^A(t) \right\| \leq \varepsilon_R$, where ε_R is the desired accuracy of the rotation matrix.

5.2. Estimation of translational errors. Once the rotation matrices are corrected, these results would be then used to calculate translational errors. By using the actual value of μ_k, R_A^P and R_H^A, the translational error's Jacobian matrix J_T in the translational error model (12) can be calculated based on (9). J_T is the rank deficient and it can be written as:

$$J_T = V_t \Sigma_t U_t \qquad (34)$$

$$\Sigma_t = \begin{bmatrix} \lambda_1 & \cdots & 0 & \cdots & 0 \\ \vdots & \ddots & \vdots & \ddots & \vdots \\ 0 & \cdots & \lambda_i & \cdots & 0 \\ \vdots & \cdots & \vdots & \ddots & \vdots \\ 0 & \cdots & 0 & \cdots & 0 \end{bmatrix} \qquad (35)$$

where V_t and U_t are orthonormal matrices and $\lambda_i (i \leq 5)$ are the nonzero singular values of J_t.

By using the pseudo inverse of Σ_t denoted by Σ_t^+, translational errors $\Delta^P p_A^P$ and $\Delta^H p_E^H$ are estimated as:

$$col(\Delta^P p_A^P, \Delta^H p_E^H) = U_t^T \Sigma_t^+ V_t^T \rho_t. \qquad (36)$$

5.3. Verification method. The verification method is designed in this section to verify the calibration results. Ma [13] verified the calibration results by computing the closeness of the left and right side of the equation $\mathbf{AXB} = \mathbf{YCZ}$. In our paper, inspired by [13], we evaluate the base-base and hand-eye calibration results by comparing the mismatch errors before and after dual robot calibration. The mismatch errors are the distances between the positions of the feature point and the constructed optical axis.

The position ${}^P p_T^P$ of the feature point is calculated by means of passive robot kinematics and tool-flange transformation. The nominal position of the camera ${}^P \bar{p}_E^P$ and the nominal value of the optical axis vector ${}^P \bar{z}_E$ are:

$$\begin{aligned}{}^P \bar{p}_E^P = \bar{R}_A^P R_H^{A \; H} \bar{p}_E^H + \bar{R}_A^{P \; A} p_H^A + {}^P \bar{p}_A^P \end{aligned} \qquad (37)$$

$$\begin{aligned}{}^P \bar{z}_E = \bar{R}_A^P R_H^{A \; H} \bar{z}_E. \end{aligned} \qquad (38)$$

The mismatch error e_b before the calibration process is:

$$e_b = \frac{\left\| ({}^P p_T^P - {}^P \bar{p}_E^P) \times {}^P \bar{z}_E \right\|}{\left\| {}^P \bar{z}_E \right\|}. \qquad (39)$$

After calibration, the estimated position of the camera ${}^P p_E^P$ and the estimated value of the optical axis vector ${}^P z_E$ are:

$$\begin{aligned}{}^P p_E^P = R_A^P R_H^{A \; H} p_E^H + R_A^{P \; A} p_H^A + {}^P p_A^P \end{aligned} \qquad (40)$$

$$\begin{aligned}{}^P z_E = R_A^P R_H^{A \; H} z_E \end{aligned} \qquad (41)$$

where $R_A^P = \bar{R}_A^P + \Delta R_A^P$, $^H p_E^H = {}^H \bar{p}_E^H + \Delta^H p_E^H$ and ${}^P p_A^P = {}^P \bar{p}_A^P + \Delta^P p_A^P$ are the calibrated actual values.

The mismatch error e_a after the calibration process is:

$$e_a = \frac{\left\| ({}^P p_T^P - {}^P p_E^P) \times {}^P z_E \right\|}{\left\| {}^P z_E \right\|}. \qquad (42)$$

From (39) and (42), it is easy to see that the mismatch error is related to all of the calibrated parameters, including rotational and translational matrices. In order to demonstrate the effectiveness of the proposed calibration method, the measurement data, which are different from the experiment data, are used in the verification experiment. Because of the randomness of the validation data, it can be proved that the accuracy of the dual manipulator system is improved if the mismatch error is decreased following calibration.
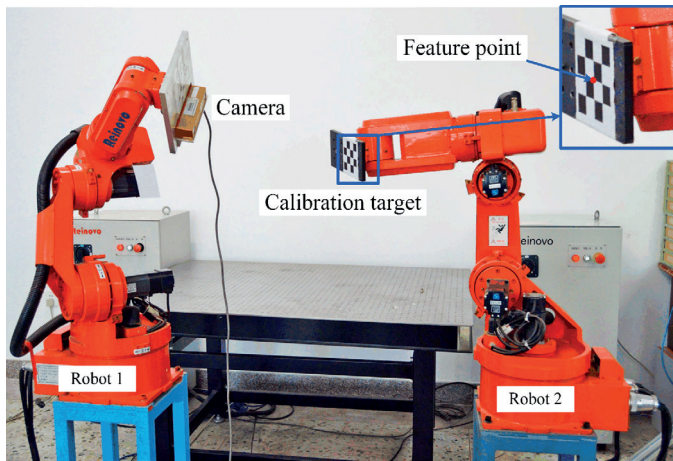
Fig.4. Configuration of the dual manipulator calibration system

6. Experiment and results

6.1. Experimental setup and initial setting. As shown in Fig. 4, the experimental setup consists of two Reinovo 6-DOF industrial manipulators, a Bumblebee CCD camera and a calibration target. The Reinovo robot has repeatability of 0.1 mm. The camera has a resolution of 1024×768 and a focal length of 2.5 mm. The calibration target is a 3×3 planar checkerboard pattern. The middlemost corner of the checkerboard pattern is chosen as the feature point.

The kinematic parameters of the two robots are shown in Table 1 and Table 2, respectively. The improved DH model [24]

Table 1
Kinematic parameter errors calibrated for the first robot

Link i	$\alpha_i(°)$	$a_i(mm)$	$d_i(mm)$	$\theta_i(°)$	$\beta_i(°)$
1	89.97	105.9	136.5	-0.15	/
2	0.26	287.8	/	89.89	0.05
3	89.66	121.4	4.7	0.37	/
4	−90.59	−0.2	312.3	−0.49	/
5	89.63	−2.1	−1.2	−90.33	/
6	0	60	123.7	−0.14	/
7	0	0.1	2.2	−90	/

Table 2
Kinematic parameter errors calibrated for the second robot

Link i	$\alpha_i(°)$	$a_i(mm)$	$d_i(mm)$	$\theta_i(°)$	$\beta_i(°)$
1	90.35	105.7	136.5	−1.37	/
2	−0.53	289.0	/	89.90	0.52
3	90.58	124.5	-3.6	−0.29	/
4	−91.10	−0.1	313.6	−1.51	/
5	91.21	1.0	0.7	−91.35	/
6	0	60.4	133.8	−0.48	/
7	0	0.5	2.8	−90	/

is used for kinematic calibration. The joint angle θ_i, link offset d_i, link length a_i, link twist α_i and rotation angle β_i are the kinematic parameters in the improved DH model. The detailed description of this non-standard DH convention is presented in the Appendix. The base-base transformation matrix $^P T_A^P$ and the hand-eye transformation matrix $^H T_E^H$ are inaccurate and have a nominal value given by:

$$^P T_A^P = \begin{bmatrix} -1 & 0 & 0 & 1200 \\ 0 & -1 & 0 & 0 \\ 0 & 0 & 1 & 0 \\ 0 & 0 & 0 & 1 \end{bmatrix}, \quad ^H T_E^H = \begin{bmatrix} 1 & 0 & 0 & -60 \\ 0 & 1 & 0 & 60 \\ 0 & 0 & 1 & 26 \\ 0 & 0 & 0 & 1 \end{bmatrix}.$$

6.2. Experiment procedure. The data measurement procedure based on the visual control method is implemented on a PC under Visual C++. The closed-loop control of the visual control method is at 10 Hz, enabling the feature point to move to the optical axis automatically and quickly. During the visual control process, the Open CV library is used to preprocess the image captured by the camera and extract the chessboard corners. The sub-pixel corner detection is an excellent technique in Open CV. The pixel coordinates of the feature point are detected in real time. An image visible in the view of the camera during the visual control process is presented in Fig. 5. The center of the red circle is the center of the optical axis, and the center of the green circle is the feature point.
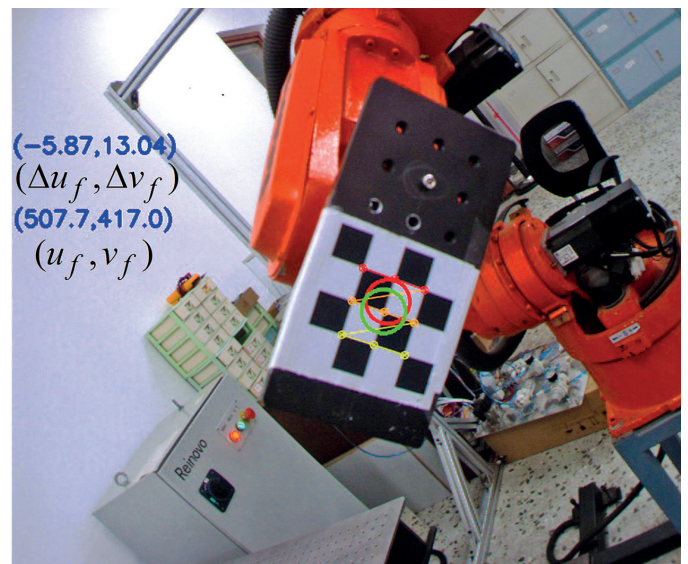

Fig.5. Sampled image in the view of camera during visual control process

During the calibration poses selection process, the directions of the optical axis have to be different from each other. They should also occupy a massive part of the operational space which is shared by the two robots to enhance observability of the errors. There are seven constructed virtual

constraints, and four positions of the feature point align with each virtual constraint. The generated calibration poses of the two robots are depicted in Fig. 6. The minimum angle $\alpha_{\min}$ in (13) is set as 45°, and the maximum angle $\alpha_{\max}$ is set as 135°. Visibility of the calibration target is best when $\alpha_v = 90°$. The distances L_v between the feature point and camera in (14) are ranging from 30 cm to 50 cm to ensure good visibility of the feature point.
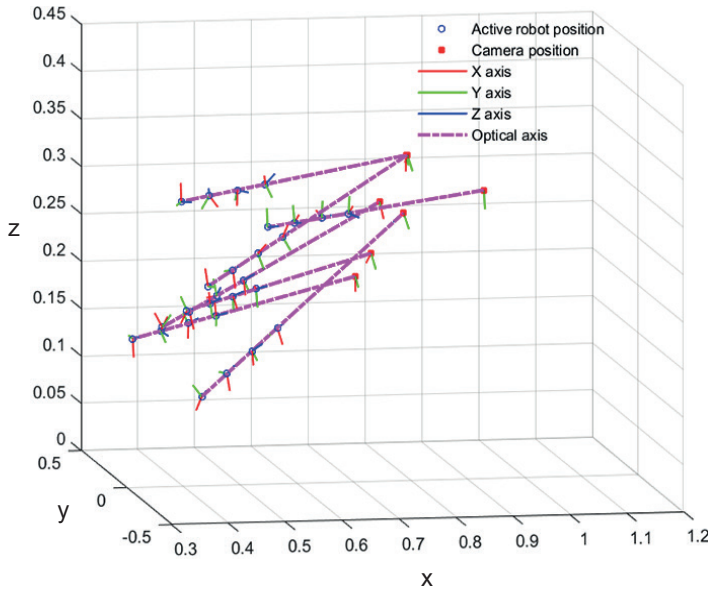

Fig. 6. The generated calibration poses of the two robots

The goal of the visual control method is to make the feature point move as close to the optical axis as possible. During the visual control process, the positioning of the calibration target is invariant. Therefore, the angle between the optical axis and calibration target has no effect on the calibration result. The feature point is supposed to align with the optical axis when the pixel difference between them is less than $[0.1, 0.1]$, with the maximum alignment error amounting to $e_{c\max} = 0.087$ mm, which is calculated based on (17, 18). Actually, the distribution of the position errors while the feature point is aligning with the optical axis at multi-positions could be approximated by a Gaussian distribution whose mean value is 0. Therefore, it can be considered that the feature point alignment errors have little influence on calibration accuracy.

6.3. Results and discussion. After the measurement procedure, the values of T_F^P, T_H^A, T_T^F and μ_k are obtained. Then the base-base rotational error ΔR_P^A and optical axis direction error $\Delta^H z_C$ of the robots are calibrated firstly by using the iterative algorithm described in section 5.1. The estimated values of ΔR_P^A and $\Delta^H z_C$ at each iteration are converged quickly, as shown in Fig. 7. The recursive error of ΔR_P^A reduces from 0.16 to less than 0.01 after only 20 iterations. For simplicity, vector $\omega = [\omega_x, \omega_y, \omega_z]^T$ is used to denote the base-base rotational error and ΔR_P^A can be calculated based on (19) and (29–31). The
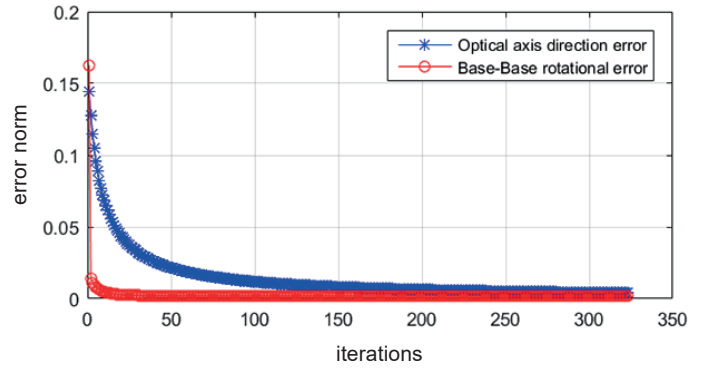

Fig.7. Recursive estimation of the base-base rotational error and optical axis direction error

estimation results of ω and $\Delta^H z_C$ are summarized in Table 3, with $\Delta^H z_C = [\Delta^H z_C(x), \ \Delta^H z_C(y), \ \Delta^H z_C(z)]^T$.

After correcting rotational errors, the resulting rotational matrices are used to estimate translational errors, as described in section 5.2. The estimation results of translational errors,

$$\Delta^P p_A^P = [\Delta^P p_A^P(x), \ \Delta^P p_A^P(y), \ ^P p_A^P(z)]^T \text{ and}$$

$$\Delta^H p_E^H = [\Delta^H p_E^H(x), \ \Delta^H p_E^H(y), \ ^H p_E^H(z)]^T,$$

are summarized in Table 4.

From Table 3 and Table 4, it could be noticed that rotational errors and translational errors of the base-base are larger than that of the hand-eye transformation. This is because initial value of the base-base transformation matrix is approximated poorly. Even though the initial errors are large, the proposed algorithm can estimate the errors recursively and achieve satisfactory accuracy.

Table 3
Estimation results of ω and $\Delta^H z_C$

Estimation of ω		Estimation of $\Delta^H z_C$	
Error variable	Estimated error	Error variable	Estimated error
ω_x	-0.0122	$\Delta^H z_C(x)$	-0.0978
ω_y	0.0805	$\Delta^H z_C(y)$	-0.0076
ω_z	-0.1579	$\Delta^H z_C(z)$	-0.0001

Table 4.
Estimation results of $\Delta^P p_A^P$ and $\Delta^H p_E^H$

Estimation of $\Delta^P p_A^P$		Estimation of $\Delta^H p_E^H$	
Error variable	Estimated error (mm)	Error variable	Estimated error (mm)
$\Delta^P p_A^P(x)$	18.2	$\Delta^H p_E^H(x)$	7.3
$\Delta^P p_A^P(y)$	113.0	$\Delta^H p_E^H(y)$	-6.8
$^P p_A^P(z)$	11.5	$^H p_E^H(z)$	-0.57

6.4. Experimental validation. Verification experiments are performed to demonstrate the effectiveness of the proposed method. In the verification experiments, the data measurement procedure is repeated. Two virtual constraints are constructed and seven positions of the feature point align with each virtual constraint. The mismatch errors before and after base-base and hand-eye calibration are depicted in Fig. 8.
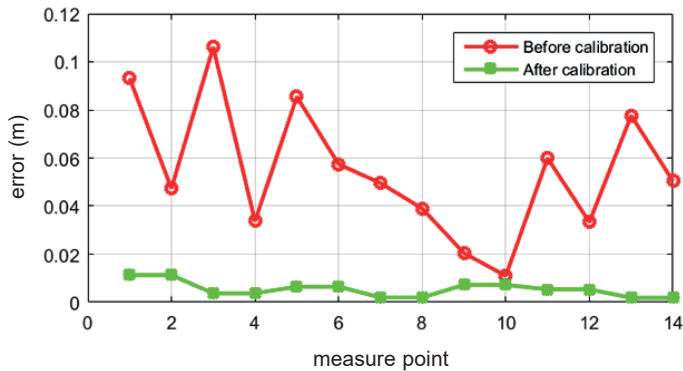

Fig. 8. Mismatch errors between optical axis vectors before and after calibration

The maximum mismatch error reduces from 106.1 mm to 11.3 mm, and the average mismatch error reduces from 60.8 mm to 6.2 mm, i.e. by as much as 89.8%. The comparison of the mismatch errors shows that the accuracy of the dual manipulator system is improved by using the method proposed.

7. Discussion

Generally, laser and optical sensors could be used to replace the camera and calibration target used in this paper. A laser is used to construct the virtual constraint and an optical sensor is centered on the laser line. Newman [25] used the laser constraint to calibrate robot kinematic parameters. The laser constraint and optical axis constraint are compared from the following aspects:

1) **Cost.** Laser has a slightly lower cost as compared to the high resolution camera. Their costs are positively correlated with their accuracy. Still, both of them are very cheap as compared to high precision devices such as laser tracker and the optical capture system. However, cameras are more often used in robot tasks nowadays and they have become almost standard features in robots.

2) **Convenience.** Thanks to extensive research on robot vision, the vision-based robot control method has been greatly developed. It is convenient for detecting the corners of the calibration target and automatically controlling the movement of the robot based on the visual control algorithm. Therefore, the calibration process based on the optical axis constraint is more automatic and convenient.

3) **Accuracy.** For the laser-based calibration method, the calibration results depend on the spot size of the laser beam. Generally, the spot size of the high precision laser is less

than 0.2 mm when the distance between the laser and optical sensor is 0.5 m. For the camera-based calibration method, the calibration results depend on the corner detection accuracy. Take the camera used in our experiments as an example: the detection error is 0.087 mm when the distance between the camera and the calibration target is 0.5 m.

As a consequence, the accuracy of the camera used in our experiment is slightly higher than that of the laser. The detection error will become even smaller if the camera has higher resolution.

8. Conclusions

A virtual constraint-based calibration method for a dual manipulator system is proposed in this paper. It is inexpensive and easy to perform. The main contributions of our efforts to this paper are as follows: (1) The robot-robot and hand-eye matrices of the dual manipulator system can be calibrated simultaneously using the proposed method. (2) The measurement process is completed automatically, which simplifies the calibration process. (3) The iterative estimation algorithm is designed to estimate the parameter errors and does not require 3D pose measurement. The average mismatch error is decreased by 89.8%, which verifies the effectiveness of the proposed method.

Combined with our previous work, i.e. [21], the dual manipulator system, including the kinematics, the relationship of robot-robot, hand-eye and flange-tool can be calibrated by using only a camera and calibration target. However, the relative rotational errors of the hand-eye configuration are only calibrated partially. Our future work will focus on solving this problem and correct the hand-eye rotational matrix fully. The proposed virtual constraint-based calibration method will be extended to include the single-manipulator and multi-manipulator systems. Moreover, we will pay more attention to calibration poses optimization and study its influence on calibration results thoroughly.

Nomenclature

A	base frame of active robot
P	base frame of passive robot
H	end-effector frame of active robot
F	end-effector frame of passive robot
E	camera frame
T	marker target frame
T_Y^X	homogeneous transformation matrix from frame Y to frame X
R_Y^X	rotation matrix from frame Y to frame X
$^Z p_Y^X$	relative position vector from origin of frame Y to origin of frame X in frame Z
$^X z_Y$	vector of Z-axis of frame Y in frame X
$P_c^{(k)}$	origin of the camera frame

$^A\boldsymbol{P}_e^{(i,k)}$　calibration position of the feature point in the active robot base frame

$^P\boldsymbol{P}_e^{(i,k)}$　calibration position of the feature point in the passive robot base frame

α_v　angle between the optical axis and the calibration target

L_v　distance between the camera and the calibration target

$\boldsymbol{\theta}$　vector of robot joint angles

θ_v　scalar value related to v

$\boldsymbol{v}$　unit vector

$S(\bullet)$　cross-product matrix of vector

$\overline{\bullet}$　nominal value

$\Delta\bullet$　error between nominal value and true value

$\delta\bullet$　small error of matrix

$\boldsymbol{\mu}_k$　vector of the kth optical axis

$\bullet^{(i,k)}$　matrix at the kth virtual constraint and the ith position of the feature point

$\boldsymbol{J}_T$　translational error's Jacobian matrix

$\boldsymbol{\rho}_t$　translational error matrix

$\boldsymbol{J}_R$　rotational error's Jacobian matrix

$\boldsymbol{\rho}_R$　rotational error matrix

n　total number of virtual constraints

m　total number of positions of the feature point at each virtual constraint

t　number of iterations

ε_R　desired accuracy of rotational matrix

θ_i　joint angle of the ith link

d_i　link offset of the ith link

a_i　link length of the ith link

α_i　link twist of the ith link

β_i　rotation angle of the ith link

eb　mismatch error before the calibration process

e_a　mismatch error after the calibration process

$e_{c\max}$　maximum value of the poses alignment error

Appendix

The kinematics model for robot calibration should meet the following conditions: model completeness, parameter minimality and model continuity. In the DH method, the kinematic model is not continuous for the robots which possess parallel or near-parallel joint axes. Hayati [24] proposed an improved DH model. For the general joint axes, DH method is applied for robot kinematic modeling. The DH model is standard thus its details are not presented here. For the parallel or near-parallel consecutive joint axes, an additional parameter β is added to describe the deviation between the parallel axes.

As shown in Fig. 9, β take the form of rotations around y axes to align the z axis with that of joint $i+1$. The transformation between the i and $i+1$ coordinate axes is:

$$^i\boldsymbol{T}_{i+1} = \begin{bmatrix} c_{\theta_i}s_{\beta_i} - s_{\theta_i}s_{\alpha_i}c_{\beta_i} & -s_{\theta_i}c_{\alpha_i} & c_{\theta_i}s_{\beta_i} + s_{\theta_i}s_{\alpha_i}c_{\beta_i} & a_i c_{\theta_i} \\ s_{\theta_i}c_{\beta_i} - c_{\theta_i}s_{\alpha_i}s_{\beta_i} & c_{\theta_i}c_{\alpha_i} & s_{\theta_i}s_{\beta_i} - c_{\theta_i}s_{\alpha_i}c_{\beta_i} & a_i s_{\theta_i} \\ -c_{\alpha_i}s_{\beta_i} & s_{\alpha_i} & s_{\alpha_i}c_{\beta_i} & 0 \\ 0 & 0 & 0 & 1 \end{bmatrix}.$$
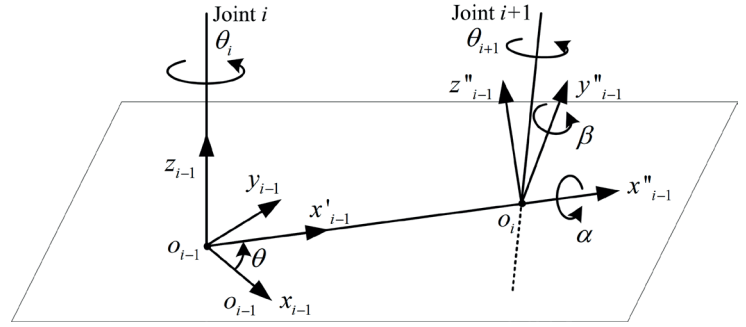
Fig. 9. Link coordinates for the near-parallel revolute joints

REFERENCES

[1] J. Vangal-Ramamurthy, R. Vasudevan, and R. Perez, "Method and devices for picking and placing workpieces into devices under manufacture using dual robots", *U.S. Patent Application* 10(39), 219 (2018).

[2] P. Aivaliotis, G. Michalos, and S. Makris, "Cooperating robots for fixtureless assembly: modelling and simulation of tool exchange process", *International Journal of Computer Integrated Manufacturing* 31(12), 1235–1246 (2018).

[3] C. Zieliński and T. Winiarski, "General specification of multi-robot control system structures", *Bull. Pol. Ac.: Tech.* 58(1), 15–28 (2010).

[4] W. Wang, H. Song, Z. Yan, and L. Sun, "A universal index and an improved PSO algorithm for optimal pose selection in kinematic calibration of a novel surgical robot", *Robotics and Computer-Integrated Manufacturing* 50, 90–101 (2018).

[5] I. Duleba and I. Karcz-Duleba, "Suboptimal approximations in repeatable inverse kinematics for robot manipulators", *Bull. Pol. Ac.: Tech.* 65(2), 209–217, (2017).

[6] Y. Meng and H. Zhuang, "Autonomous robot calibration using vision technology", *Robot. Comp. Integr. Manuf* 4(23), 436–446 (2007).

[7] F. Dornaika and R. Horaud, "Simultaneous robot-world and hand-eye calibration", *IEEE Trans. Robot. Autom* 14(4), 617–622 (1998).

[8] W. Wang, F. Liu, and C. Yun, "Calibration method of robot base frame using unit quaternion form", *PrecisionEng*, 41, 47–54 (2015).

[9] A. Li, L. Wang, and D. Wu, "Simultaneous robot-world and hand-eye calibration using dual-quaternions and Kronecker product", *Int. J. Phys. Sci.* 5(10), 1530–1536 (2010).

[10] M. Shah, "Solving the robot-world/hand-eye calibration problem using the Kronecker product", *J. Mech.Robot.*, 5(3), 031007, 2013.

[11] J. Heller, D. Henrion, and T. Pajdla, "Hand-eye and robot-world calibration by global polynomial optimization". Proceedings of IEEE International Conference Robotics Automation (ICRA), 30, pp. 3157–3164, 2014.

[12] L. Wu, J. Wang, L. Qi, K. Wu, H. Ren, and M.Q.H. Meng, "Simultaneous hand-eye, tool-flange, and robot–robot calibration for comanipulation by Solving the AXB = YCZ Problem", *IEEE Trans. Robot.* 32 (2), 413–428 (2016).

[13] Q. Ma, Z. Goh, S. Ruan, and G.S. Chirikjian, "Probabilistic approaches to the AXB = YCZ AXB = YCZ calibration problem in multi-robot systems", *Autonomous Robots* 42, 1497–1520 (2018).

[14] G. Du and P. Zhang, "Online robot calibration based on vision measurement", *Robot. Comp. Integr. Manuf.* 29, 484–492 (2013).

[15] H. Wang, X. Lu, Z. Hu, and Y. Li, "A vision-based fully-automatic calibration method for hand-eye serial robot", *Ind. Robot* 42(1), 64–73 (2015).

[16] Y.H. Gan and X.Z. Dai, "Base frame calibration for coordinated industrial robots", *Robot. Auton. Syst.* 59, 563–570 (2011).

[17] H. Deng, H. Wu, C. Yang, Y. Guan, H. Zhang, and J. Liu, "Base frame calibration for multi-robot coordinated systems". Proceedings of the 2015 IEEE Conference on Robotics and Biomimetics, Zhuhai, China, December 6–9, 2015.

[18] R.G. Bonitz and T.C. Hsia, "Calibrating a multi-manipulator robotic system", *IEEE Robot. Autom. Mag* 4(1), 18–22 (1997).

[19] R.L. Hirsh, G.N. DeSouza, and A.C. Kak, "An iterative approach to the hand-eye and base-world calibration problem". Proceedings of IEEE International Conference on Robotics and Automation, 3, pp. 2171–2176, 2001.

[20] D. Wu and H. Ren, "Finding the kinematic base frame of a robot by hand-eye calibration using 3D position", *IEEE Trans. Autom. Sci. Eng.* 99, 1–11 (2016).

[21] Q. Zhu, X. Xie, C. Li, G. Xia, and Q. Liu, "Kinematic Self-Calibration Method for Dual-Manipulators Based on Optical Axis Constraint", *IEEE Access* 7, 7768–7782 (2019).

[22] A. Joubair and I.A. Bonev, "Comparison of the efficiency of five observability indices for robot calibration", *Mechanism & Machine Theory*, 70, 254–265 (2013).

[23] G. Taubin, "3D Rotations", *IEEE computer graphics and applications*, 31(6), 84–89 (2011).

[24] S.A. Hayati, "Robot arm geometric link parameter estimation," in *The 22nd IEEE Conf. Decision and Control*., 1477–1483 (1983).

[25] W.S. Newman and D.W. Osborn, "A new method for kinematic parameter calibration via leser line tracking", in *IEEE Int. Conf. Robotics and Automation*, Atlanta, USA. 160–165, 1993.